Phys Chem Minerals (2003) 30: 280 – 292
DOI 10.1007/s00269-003-0319-1
© Springer-Verlag 2003

ORIGINAL PAPER

C. A. Geiger · M. Grodzicki · G. Amthauer

The crystal chemistry and Fe^{II}–site properties of aluminosilicate garnet solid solutions as revealed by Mössbauer spectroscopy and electronic structure calculations

Received: 29 July 2002 / Accepted: 10 March 2003

Abstract The three binary garnet solid solutions $Fe_3^{II}Al_2Si_3O_{12}$–$X_3^{II}Al_2Si_3O_{12}$ ($X^{II} = Mg^{II}$, Mn^{II}, Ca^{II}) have been investigated by ^{57}Fe Mössbauer spectroscopy at 298 and 77 K and by electronic structure calculations in the local spin density approximation. The spectra yield isomer shifts and quadrupole splittings that are typical for Fe^{II} in the dodecahedral X-site of 222 point symmetry and are similar for each of the three binaries recorded. Conversely, electronic structure calculations based on the experimental crystal structure of the different end-member garnets exhibit pronounced variations in some of the electronic properties of Fe^{II} that are not reflected in the spectroscopic data. These results are interpreted as indicating that the different X–O bonds in garnet solid solutions retain to a large degree the intrinsic lengths that they possess in their respective end members, and that the Fe–O bond does not change greatly as a function of composition. This is evidence for the state of alternating bonds and not for the virtual crystal approximation in describing the X–O bond types or lengths in aluminosilicate garnet solid solutions. The observed degree and behavior of the Fe^{II} doublet asymmetry in the Mössbauer spectra for the three solid solution series do not indicate major variations in the anisotropic recoil-free fraction of Fe^{II}. Variations in doublet asymmetry are more likely a result of complex next-nearest X-site neighbor interactions and/or some degree of short-range cation ordering, though doublets representing different local X-site cation configurations cannot be resolved or fitted to the experimental spectra.

C. A. Geiger (✉)
Institut für Geowissenschaften,
Universität Kiel Olshausenstr. 40,
24098 Kiel, Germany
Tel.: +49-431-880-2895
Fax: +49-431-880-4457
e-mail: chg@min.uni-kiel.de

M. Grodzicki · G. Amthauer
Institut für Mineralogie,
Universität Salzburg Hellbrunner Str. 34, 5020 Salzburg, Austria

Keywords Garnet · Mössbauer spectroscopy · Solid solutions · Electronic structure calculations · Site relaxation

Introduction

While the microstructural and macroscopic properties of end-member silicates are relatively well known, it is poorly understood how atomistic level properties govern the energetics, *P–T* stabilities, and bulk physical properties of solid solutions. Local atomistic structural properties of a solid solution can often be measured only with difficulty, and it is not a simple matter to relate them to the macroscopic physical properties that represent the sum of all local states. Consequently, the interpretation of such data is based on certain assumptions whose significance is not completely clear. On the one hand, it is sometimes assumed in mineralogical investigations that experimental bond lengths of a given site, as determined by diffraction methods, vary monotonically as a function of composition across a binary solid solution, for example. This has been described as the virtual crystal approximation (VCA; Martins and Zunger 1984; Urusov 2001). On the other hand, it is generally accepted that atomic radii remain approximately constant from structure to structure or over a range of compositions. Thus, the element-specific bonds largely retain the length and character in the solid solution that they have in their respective end members. In the case of alloys and semiconductors, this situation has been described as the state of alternating bonds (Martins and Zunger 1984). The two situations are obviously contradictory, and little has been done, at least in the field of silicates, in the way of trying to determine which model provides the proper description for solid solutions.

Spectroscopic measurements provide the best opportunity to look at local and/or element-specific bonding, and here Mössbauer spectroscopy can be quite useful. It delivers information in the case of the ^{57}Fe

nucleus only on the Fe–O bonding through measurement of the hyperfine parameters. The silicate solid solution chosen for such a study in this paper is that of the aluminosilicate garnets. It provides an optimal system for investigation because Fe^{II} substitution occurs on a single site and solid solution occurs over a wide range of composition. The first detailed Mössbauer studies of iron in the different polyhedral sites in garnet go back to the 1970s (Lyubutin and Lyubutina 1971; Lyubutin and Dodokin 1971; Amthauer et al. 1976). These investigations showed that both isomer shifts, δ, and quadrupole splittings, ΔE_Q, of Fe^{II} in the dodecahedral X-site are large with $\delta \approx 1.30\,mm^{-1}s$ and $\Delta E_Q = 3.5$–$3.6\ mm\ s^{-1}$, respectively, at 298 K. These values belong to the highest reported ones for ferrous iron in crystalline oxides or silicates, and have been interpreted as indicating a high degree of ionic bonding (Evans and Sergent 1975; Amthauer et al. 1976). Amthauer et al. (1976) carried out a detailed analysis of the electric-field gradient tensor for the different polyhedral sites and made estimations of their corresponding Debye temperatures in natural garnets over a wide range of composition. They also determined the sign of the electric-field gradient of Fe^{II} in the dodecahedral X-site in an external magnetic field to be negative over the temperature range of 4 to 1000 K, and to be insensitive to the magnitude of the asymmetry parameter η. The most direct information about Fe–O bonding can, of course, be obtained from electronic structure calculations. However, to the best of our knowledge, no reliable calculations on the electronic structure and spectroscopic properties of Fe-bearing garnets have been published.

In this paper, ^{57}Fe Mössbauer spectra of the three synthetic garnet solid-solution binaries $Fe^{II}_3Al_2Si_3O_{12}$ – $X^{II}_3Al_2Si_3O_{12}$ ($X^{II} = Mg^{II}$, Mn^{II}, Ca^{II}), i.e., almandine (Alm) with pyrope (Pyr), spessartine (Spe), and grossular (Gro), respectively, have been measured to address three issues. First, systematic measurements were undertaken on compositionally simple and structurally well-characterized synthetic solid solutions to probe for variations in Fe–O bonding and local structural properties at length scales shorter than those delivered by standard diffraction methods. This was done to investigate dodecahedral X-site properties accompanying changes in garnet composition, since it is not yet clear how the X–O bonding types vary as a function of garnet composition. Inferences have been made based on simple crystal chemical arguments and diffraction results (Ungaretti et al. 1995; Geiger and Feenstra 1997), but they are, at this point, largely qualitative in nature. According to previous Mössbauer results on natural garnets, such variations are expected to be small, if existent at all (e.g., Amthauer et al. 1976; see, however, Ungaretti et al. 1995). In natural garnets, however, which are compositionally complex and have experienced complicated thermal and geologic histories, small variations in the hyperfine parameters could be masked or difficult to detect. Second, the nature of the vibrational behavior of Fe^{II} was also investigated. It has been shown for end-member almandine that the Fe^{II} cation is dynamically disordered and vibrates in a strongly anisotropic manner (Geiger et al. 1992). This effect needs to be studied in solid solution garnets and Mössbauer measurements can deliver information on whether static subsite or dynamic disorder of the Fe^{II} cation is present in the X-site of 222 point symmetry (e.g., Murad and Wagner 1987; Geiger et al. 1992; Geiger 1999). Third, the spectra were used to investigate the possibility of short-range cation ordering in the solid solutions. This is important for an understanding of the thermodynamic mixing properties and an interpretation of the calorimetric measurements made on garnet solid solutions. Short-range order has been found for Mg and Ca in Pyr–Gro solid solutions using ^{29}Si NMR spectroscopy (Bosenick et al. 1995, 1999) and it is necessary to investigate the possibility of it in almandine-containing garnets. Finally, the Mössbauer measurements have been supplemented by electronic structure calculations in the local spin density approximation (LSDA) based on the experimental structures of the different garnet end members (i.e., Alm, Pyr, Gro, and Spe). Both approaches, together, offer the possibility to reveal the properties of the dodecahedral Fe site in garnet solid solutions.

Experimental and theoretical methods

The synthesis conditions and the characterization of the garnet solid solutions studied in this work have been described several times (Geiger et al. 1987, 1989; Geiger and Feenstra 1997; Kolesov and Geiger 1998; Geiger 1998). Regarding the synthesis conditions, all garnets were prepared using glass starting materials and were synthesized dry in a piston-cylinder device at elevated pressures and temperatures. The Alm-Pyr/Gro garnets were made from mechanical mixtures of the end-member glasses (Geiger et al. 1987), while the Alm–Spe garnets were synthesized from homogeneous glasses (Geiger and Feenstra 1997). The former binaries are characterized by a certain degree of compositional inhomogenity as revealed by microprobe analysis.

Six Alm–Pyr and five Alm–Spe garnet solid solution compositions were measured at 293 and 77 K in Kiel, and three Alm–Gro garnets were measured in Salzburg. In Kiel, ground garnet powders were pressed together with corn starch into pellets of diameter 12.0 mm with approximately 5 mg $Fe^{II}\ cm^{-2}$. Mirror-image spectra were collected on a 1024-multichannel analyzer and then folded. The spectra were fitted with the program MÖSALZ (courtesy of W. Lottermoser, Salzburg University) using single Lorentzian lines for the Fe^{II} doublet (Geiger et al. 1992). The low-temperature measurements were made with an Oxford cryostat with the absorber held at approximately 77 K. Fe foil was used for calibration and the reported precision of the hyperfine parameters is considered better than 0.01 $mm\ s^{-1}$. The areas of the two Fe^{II} lines were determined after subtracting out the minor contribution from octahedral Fe^{III}.

The calculations have been performed in the local spin density approximation (LSDA) by the spin-polarized self-consistent charge (SCC-)$X\alpha$ method (Grodzicki 1980, 1985). However, the $X\alpha$ potential (with $\alpha = 0.7$) is used only for the evaluation of the two- and three-center integrals, while the one-center integrals are derived from all-electron (relativistic) atomic Dirac–Fock calculations. Furthermore, the core electrons enter the two- and three-center integrals via a pseudopotential also derived from relativistic atomic calculations. The method is, hence, ab initio in the sense that it does not contain any adjustable parameter. The valence basis set

consists of 2s-, 2p-orbitals for O and F, 3s-, 3p-orbitals for Mg, Al, and Si, 4s-, 4p-orbitals for Ca, and 3d-, 4s-, 4p-orbitals for Fe.

Within the framework of the LSDA, ionization and excitation energies are usually calculated by the transition state procedure (Slater 1974). In most cases, this leads to a uniform shift of all orbital energies so that energy differences are affected only to a minor extent. Accordingly, *d–d* excitation energies are determined as the respective orbital energy differences. The quadrupole splitting, ΔE_Q, is related to the components $|V_{zz}| \geq |V_{yy}| \geq |V_{xx}|$ of the electric field gradient (efg) tensor in its principal axes system by

$$\Delta E_Q = (1/2)\ e_o Q V_{zz}\ (1+\eta^2/3)^{1/2}\ , \tag{1}$$

where the asymmetry parameter $\eta = (V_{xx} - V_{yy})/V_{zz}$ can take values between 0 and 1. It describes the deviation of the efg from axial symmetry. The size of the nuclear quadrupole moment, Q, of the first excited state of ^{57}Fe is assumed to be between 0.15 and 0.17 barn (Ray and Das 1977; Lauer et al. 1979; Dufek et al. 1995; Blaha et al. 2000). Experimentally determined isomer shift differences, $\Delta\delta$, of the same Mössbauer nucleus in different chemical environments, A and B, are related to the corresponding differences of the electron densities at the Mössbauer nuclei:

$$\Delta\delta = \delta_A - \delta_B = \alpha[\rho_A(0) - \rho_B(0)]\ . \tag{2}$$

The isomer shift calibration constant, α, for ^{57}Fe covers values in the range of $(-0.25 \pm 0.03)a^3$ mm s^{-1}, according to results from nonempirical electronic structure calculations (Duff 1974; Nieuwpoort et al. 1978; Akai et al. 1986; van der Heyden et al. 1987; Zhang et al. 1987; Eriksson and Svane 1989; Jansen et al. 1992).

The calculation of the efg tensor and of the electron density at the nucleus within the framework of a valence-electron-only electronic structure calculation has been described in detail previously (Grodzicki et al. 1987; Grodzicki and Amthauer 2000). With respect to a basis set of atomic orbitals, the efg tensor can be decomposed into three different contributions, viz. the valence contribution arising from the anisotropy of the valence shell of iron, the covalence contribution describing the anisotropy of the bonding electrons between iron and the surrounding ligands, and the ligand contribution arising from the ion cores and the valence electrons of the ligands. The polarization of the core electrons of the iron atom is accounted for by the Sternheimer shielding function, $\gamma(r)$, that has been derived from atomic self-consistent first-order perturbation calculations (Lauer et al. 1979). In the principal axes system of the efg tensor, the efg V_{zz} is simply the sum of the valence, covalence, and ligand contributions, and the usually dominating valence contribution is roughly proportional to the anisotropies

$$\Delta n_d = n_{x^2-y^2} + n_{xy} - n_{z^2} - (n_{xz} + n_{yz})/2 \tag{3}$$

$$\Delta n_p = (n_x + n_y)/2 - n_z \tag{4}$$

of the Fe(3d) shell and Fe(4p) shell occupations, n_i, respectively. While it follows immediately that the anisotropy of the Fe(3d) shell dominates the efg for high-spin ferrous iron, it is often assumed that for high-spin ferric iron the ligand contribution should be the largest. However, several calculations have demonstrated that generally the valence contribution dominates even when the anisotropy should vanish according to crystal-field theory (Keutel et al. 1999; Grodzicki et al. 2000, 2001).

The central problem in calculating $\rho(0)$ is that, on one hand the amplitudes, $\varphi_{is}(0)$, of the *s*-orbitals at the Mössbauer atom require a high degree of accuracy whereas, on the other hand, the core orbitals are not included in a valence-electron-only method. For this reason, the amplitudes, $\varphi_{is}(0)$, of both the core and valence *s*-orbitals at the origin are determined for the free ion by fully numerical (i.e., basis set free) relativistic atomic calculations for a certain number of valence shell configurations. In the case of ^{57}Fe these are $4s^{n_s}3d^{n_d}$ with $n_s = 0, 1, 2$ and $n_d = 4, 5, 6, 7$ except the configuration $4s^2 3d^7$. From these 11 values an interpolation formula is derived as a function of the valence shell occupation numbers, n_s and n_d, for each atomic core and valence *s*-orbital of iron:

$$\sqrt{(4\pi)}\varphi_i^{rel}(0) = a_{io} + a_{is}n_s + a_{id}n_d + a_{iss}n_s^2 + a_{isd}n_s n_d + a_{idd}n_d^2\ . \tag{5}$$

It should be emphasized that the valence orbitals of the Mössbauer atom are included in this procedure, because the size of the basis set entering the cluster calculation is usually not sufficient, especially for large systems.

Experimental results

Preliminary results for Alm–Pyr/Gro garnets were given in Geiger et al. (1990) and those for Alm–Spe garnets in Geiger (1993). The results of this work supersede these earlier studies though without significant differences. Representative spectra recorded at 298 and 77 K are shown in Fig. 1a and b, respectively. The top row in Fig. 1a shows the spectra of three Alm–Pyr solid solutions of composition, from left to right, $Alm_{93}Pyr_{07}$, $Alm_{60}Pyr_{40}$, and $Alm_{10}Pyr_{90}$. The middle row shows three Alm–Spe solid solutions of composition $Alm_{87}Spe_{13}$, $Alm_{50}Spe_{50}$, and $Alm_{09}Spe_{91}$. The bottom row shows the spectra of three Alm–Gro solid solutions of composition $Alm_{90}Gro_{10}$, $Alm_{50}Gro_{50}$, and $Alm_{10}Gro_{90}$. Figure 1b shows the corresponding spectra at 77 K. The hyperfine parameters and line widths for all compositions studied are given in Tables 1 and 2, and confirm essentially previous results on natural aluminosilicate garnets (Amthauer et al. 1976). The quadrupole splittings measured across the three binaries at 298 and 77 K are shown in Fig. 2a and b, respectively. The quadrupole splittings of Fe^{II} are very large with 3.50–3.57 mm s^{-1} at 298 K, and with 3.63–3.71 mm s^{-1} at 77 K, and are thus in the same range as those reported for natural garnets. The isomer shift values for all compositions along the three joins are 1.27 ($\pm$ 0.01) mm s^{-1} at 298 K and 1.41 ($\pm$ 0.01) mm s^{-1} at 77 K, compared with $\delta \approx 1.30$ mm s^{-1} at 298 K for natural almandine-containing garnets. Altogether, the hyperfine parameters change little as a function of composition and the spectra of all the garnet solid solutions are similar (Fig. 1a, b).

Theoretical results

The first series of cluster molecular-orbital(MO) calculations investigates the dependence of the available spectroscopic data on the cluster size for the garnet end-member almandine. The calculations are based on its experimentally determined crystal structure at 100K (Armbruster et al. 1992). Experience from previous cluster calculations on minerals (Lougear et al. 2000; Grodzicki and Amthauer 2000; Grodzicki et al. 2001; Lottermoser et al. 2002; Grodzicki et al. 2002) has shown that reliable results for the hyperfine parameters require that at least the surroundings of each oxygen atom of the first coordination sphere of the central iron are correctly described and that large negative cluster charges are avoided. Accordingly, model calculations on a $[FeO_8]^{14-}$ cluster representing just the first coordination sphere are not expected to give reliable results for the electronic properties of ferrous iron at the X site in garnets. At least the cations of the second coordination sphere have to be included as well, comprising four divalent (Mg, Fe, Mn, Ca) and trivalent (Al) cations and six (formally tetravalent) silicon atoms.

Each of these cations is eightfold (Mg, Fe, Mn, Ca), sixfold (Al), or fourfold (Si) coordinated by oxygen atoms leading to 40 oxygen atoms in the third shell. Terminating the cluster at these oxygens gives, however, an inappropriate description of the electronic properties. First of all, the formal oxygen charge of -2 results in a large negative cluster charge that causes convergency problems if not compensated by a Madelung-type potential, e.g., of distributed point charges. Secondly, omitting the cations of the next shell bonded to the oxygens produces unsaturated O(2p)-lone-pair orbitals that are in the same energy range as the Fe(3d)-orbitals and may occasionally also cause convergency problems. Actually, both the bonding to the omitted cations and the Madelung potential will lead to a stabilization of these O(2p)-orbitals and thus would remove the convergency problems.

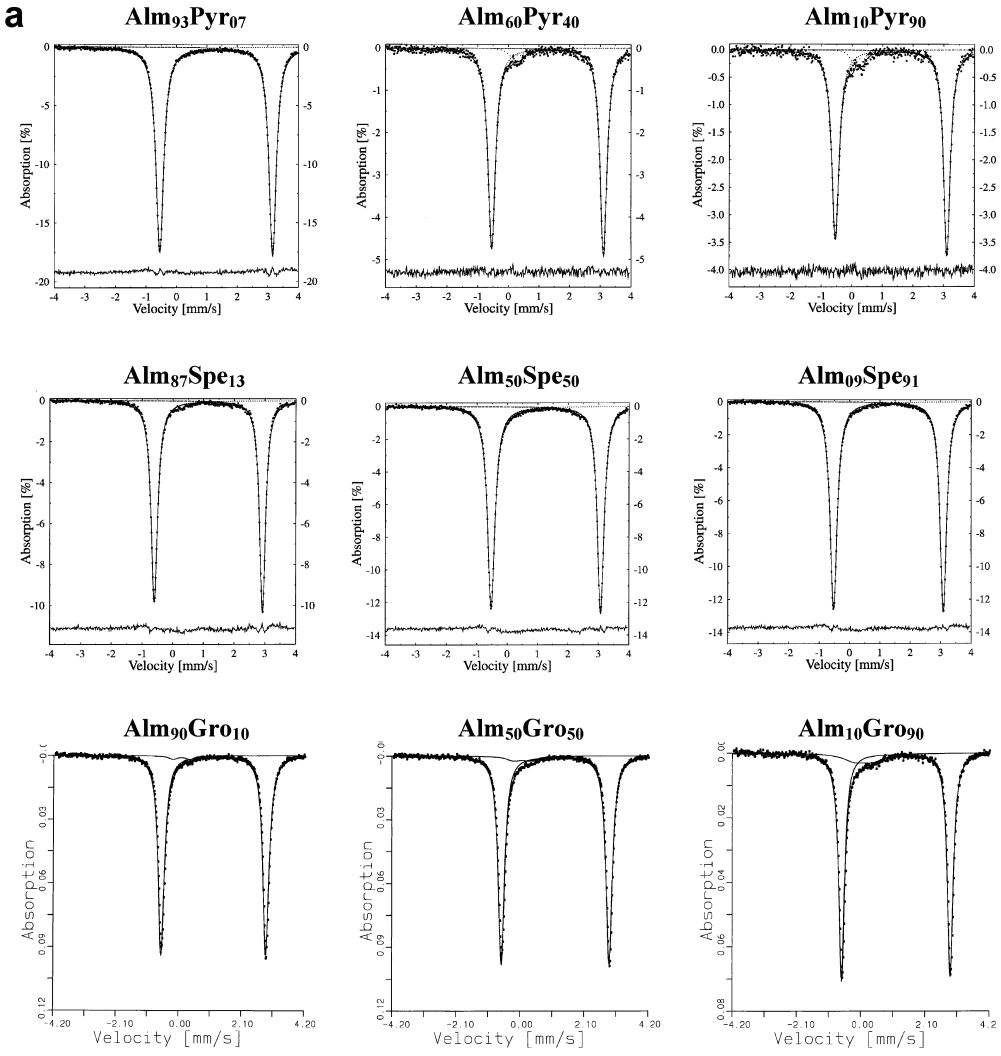

Fig. 1a, b ^{57}Fe Mössbauer spectra recorded at 298 K on the three almandine-containing garnet solid solutions. The *top row* shows the spectra of three Alm–Pyr solid solutions of composition, *from left to right*, $Alm_{93}Pyr_{07}$, $Alm_{60}Pyr_{40}$, and $Alm_{10}Pyr_{90}$. The *middle row* shows three Alm–Spe solid solutions of composition $Alm_{87}Spe_{13}$, $Alm_{50}Spe_{50}$, and $Alm_{09}Spe_{91}$. The *bottom row* shows the spectra of three Alm–Gro solid solutions of composition $Alm_{90}Gro_{10}$, $Alm_{50}Gro_{50}$, and $Alm_{10}Gro_{90}$. **b** The corresponding spectra at 77 K. The spectra were fit with two separate Lorentzian lines that were not constrained to have equal widths or areas

This stabilization can be attained, alternatively, by replacing some or all of the oxygens of the third shell with fluorine atoms, or by adding further polyhedra, though at the expense of CPU time and memory space. Accordingly, the smallest reasonable system fulfilling these requirements is the 55-atom cluster of composition $[FeO_8–Mg_4Al_4Si_6F_{32}]^{2-}$. This cluster is stepwise enlarged by replacing the fluorines of the third shell by oxygens and adding at the same time the corresponding adjacent polyhedra in such a way that the total charge of the clusters remains constant (i.e., $Q = -2$). The largest cluster constructed in this way is a 185-atom cluster of composition $[FeO_8–Mg_4Al_4Si_6O_{40}–Mg_{22}Al_{12}Si_{16}O_{24}F_{48}]^{2-}$. It comprises all atoms around the central iron within a sphere of 7.55 Å, and within a sphere of 6.60 Å all anions are correctly represented as oxygens.

The results for the quadrupole splitting and the *d–d* excitation energies are given in Table 3, where, for comparison, also two smaller clusters are included, viz. $[FeO_8]^{14-}$ and $[FeO_8–Si_2F_4H_8]^{6-}$. The calculated quadrupole splitting of -3.665 mm s^{-1} for the 185-atom cluster is in quantitative agreement with the low temperature experimental values between -3.65 mm s^{-1} and -3.71 mm s^{-1} on synthetic Alm (this work; Murad and Wagner 1987; Geiger et al. 1992) and those for natural garnets, viz. -3.66 mm s^{-1} (Amthauer et al. 1976). The same is true for the quadrupole splitting of the smallest nine-atom cluster but this result must be considered as fortuitous. First, the *d–d* excitation energies are only about half of the measured values, and second, increasing the cluster size yields first an increase of the quadrupole splitting and convergence towards the experimental value only for clusters with about 100 atoms, and then remains essentially constant for the larger clusters. The electric field gradient (efg), i.e., the principal axis of the efg tensor, is axially symmetric, i.e., $\eta < 0.06$ for all the larger clusters, and is directed along the pseudo-fourfold axis. Decomposing the efg into valence, covalence, and ligand contributions, as described above, reveals that the total efg is almost identical with the 3d valence contribution of -3.654 mm s^{-1} whereas the 4p valence ($+0.012$ mm s^{-1}), the covalence ($+0.003$ mm s^{-1}) and the ligand contributions (-0.026 mm s^{-1}) turn out to be negligible. This result demonstrates that point charge models for the description of the efg are inappropriate.

Similarly to the quadrupole splittings, the calculated *d–d* excitation energies of the spin-down 3d-orbitals for Fe^{II} in the dodecahedral X site are approximately size-converged with respect to the measured energies (last row of Table 3: averaged values from White and Moore 1972; Burns 1993; Geiger and Rossman 1994) for clusters of about 100 atoms, even though some oscillatory behaviour is still apparent for some of the larger systems. The calculated splitting pattern of the *d*-orbitals is the same for all clusters, and the ordering d_{z^2}, d_{xy}, d_{yz}, $d_{x^2-y^2}$, d_{xz} with respect to the calculated main axes system of the efg is identical with that proposed by Newman et al. (1978) and Burns (1993). This splitting pattern is easily correlated with the structural features of the first coordination sphere. The dodecahedron is compressed along the pseudo-fourfold *z* axis so that the d_{xy}-orbital is destabilized with respect to the d_{z^2}-orbital. In addition, a rhombohedral distortion connected with a compression along the *x* axis and an elongation along the *y* axis yields a stabilization of the d_{yz}–orbital and a destabilization of the d_{xz}-orbital relative to the

Fig. 1a, b (Contd.)

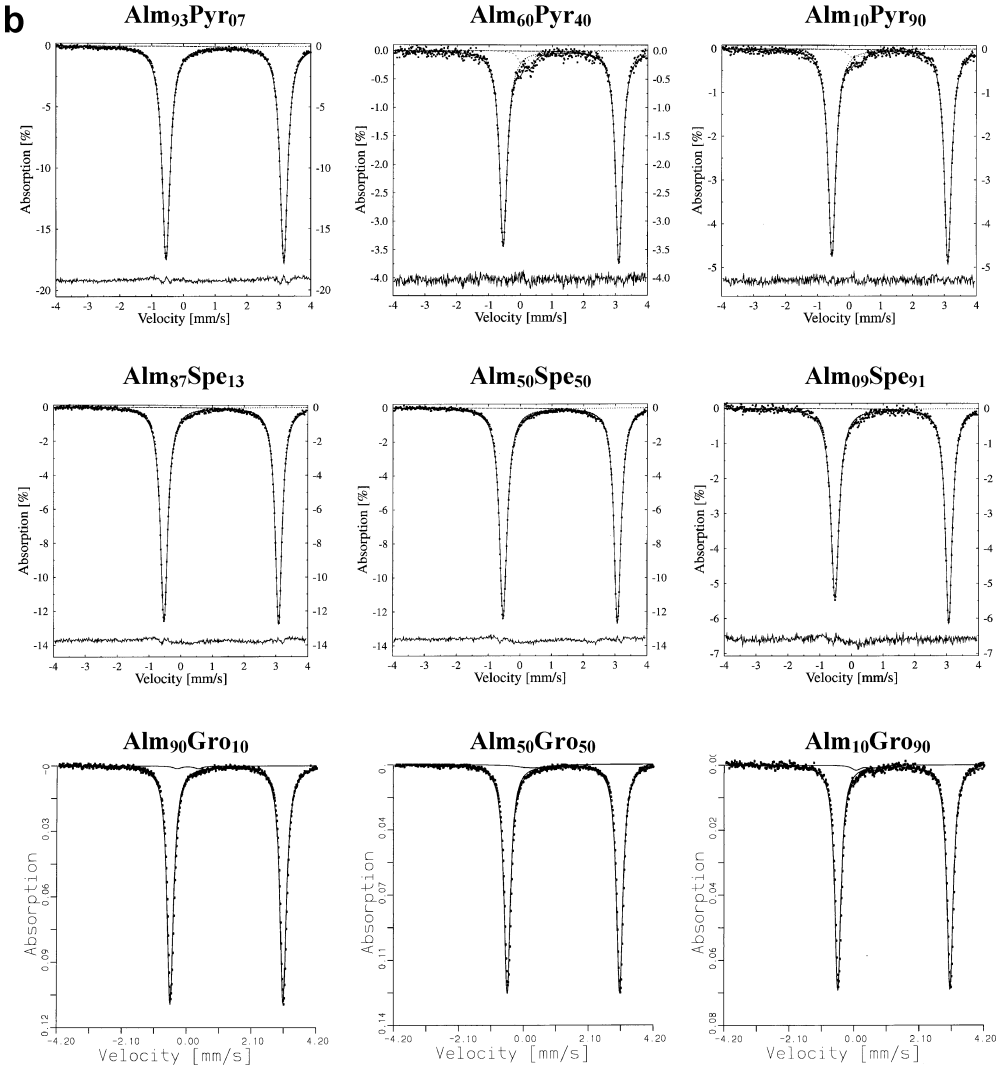

Table 1 Isomer shifts (δ), quadrupole splittings (ΔE_Q), line widths (all in mm s^{-1} with precision $\pm$ 0.01), and peak areas (in %) recorded at 298 K

Sample	δ	ΔE_Q	HW_L^a	HW_H^a	DAS^b	A_L^c	A_H^c	A_L/A_H
$Alm_{93}Pyr_{07}$	1.27	3.52	0.278	0.254	4.5	51.1	48.9	1.045
$Alm_{85}Pyr_{15}$	1.27	3.53	0.278	0.254	4.5	51.3	48.7	1.053
$Alm_{60}Pyr_{40}$	1.27	3.54	0.276	0.242	6.5	51.2	48.8	1.049
$Alm_{50}Pyr_{50}$	1.27	3.55	0.280	0.232	9.4	51.4	48.6	1.058
$Alm_{38}Pyr_{62}$	1.27	3.57	0.308	0.264	7.7	51.7	48.3	1.070
$Alm_{20}Pyr_{90}$	1.26	3.57	0.284	0.236	9.2	51.3	48.7	1.053
$Alm_{87}Spe_{13}$	1.27	3.53	0.256	0.230	5.3	51.2	48.8	1.049
$Alm_{75}Spe_{25}$	1.27	3.54	0.256	0.232	4.9	50.8	49.2	1.032
$Alm_{50}Spe_{50}$	1.28	3.55	0.266	0.234	6.4	51.6	48.4	1.040
$Alm_{25}Spe_{75}$	1.27	3.56	0.280	0.246	6.5	49.8	50.2	1.006
$Alm_{09}Spe_{91}$	1.27	3.56	0.302	0.240	11.4	51.3	48.7	1.053
Alm_{100}	1.28	3.50	0.262	0.236	5.2	50.9	49.1	1.038
$Alm_{90}Gro_{10}$	1.28	3.50	0.260	0.238	4.4	50.8	49.2	1.034
$Alm_{50}Gro_{50}$	1.27	3.53	0.268	0.236	6.9	51.6	48.4	1.068
$Alm_{10}Gro_{90}$	1.26	3.55	0.242	0.220	4.8	52.3	47.7	1.095

[a] HW_L (HW_H) = half-width of the low(high)-velocity line
[b] $DAS = 2\,\frac{HW_L - HW_H}{HW_L + HW_H} \cdot 100$
[c] A_L (A_H) = resonant absorption area of the low(high)-velocity line ($\pm$ 1.0%) referred to total resonant absorption area = 100%

$d_{x^2-y^2}$-orbital. Finally, the differences between the measured and computed energies for the cluster with 185 atoms are typical for calculations in the local density approximation yielding *d–d* excitation energies that are usually up to 20% larger.

The only significant difference occurs in the lowest *d–d* excitation energy that has been estimated from the temperature dependence of the quadrupole splitting as about 1100 cm^{-1} and is calculated about 50% too large. Therefore, the temperature dependence of the efg has been simulated (1) by accounting for the variation of the structural data with temperature (Geiger et al. 1992), and (2) by allowing thermal population of the excited orbitals proportional to the Boltzmann factor $\exp(-\delta\varepsilon/kT)$ with

Table 2 Isomer shifts (δ), quadrupole splittings (ΔE_Q), line widths (all in mm s^{-1} with precision $\pm$ 0.01), and peak areas (in %) recorded at 77 K. Notations as in Table 1

Sample	δ	ΔE_Q	HW_L	HW_H	DAS	A_L	A_H	A_L/A_H
$Alm_{93}Pyr_{07}$	1.42	3.71	0.304	0.286	6.1	51.14	48.86	1.046
$Alm_{85}Pyr_{15}$	1.42	3.71	0.300	0.276	8.3	51.44	48.56	1.059
$Alm_{60}Pyr_{40}$	1.41	3.69	0.292	0.272	7.1	50.80	49.20	1.033
$Alm_{50}Pyr_{50}$	1.41	3.69	0.280	0.254	9.7	51.00	49.00	1.041
$Alm_{38}Pyr_{62}$	1.41	3.68	0.316	0.270	15.7	51.85	48.15	1.077
$Alm_{20}Pyr_{90}$	1.40	3.68	0.290	0.260	10.9	50.47	49.53	1.019
$Alm_{87}Spe_{13}$	1.41	3.66	0.280	0.258	8.2	51.62	48.38	1.067
$Alm_{75}Spe_{25}$	1.40	3.65	0.404	0.380	6.1	51.99	48.01	1.083
$Alm_{50}Spe_{50}$	1.40	3.64	0.294	0.264	10.8	51.90	48.10	1.079
$Alm_{25}Spe_{75}$	1.40	3.64	0.348	0.304	13.5	52.29	47.71	1.096
$Alm_{09}Spe_{91}$	1.40	3.63	0.314	0.262	22.2	51.53	48.47	1.063
Alm_{100}	1.42	3.65	0.260	0.248	4.7	50.48	49.52	1.019
$Alm_{90}Gro_{10}$	1.42	3.65	0.260	0.248	4.7	50.45	49.55	1.018
$Alm_{50}Gro_{50}$	1.41	3.64	0.264	0.244	7.9	50.76	49.24	1.031
$Alm_{10}Gro_{90}$	1.40	3.63	0.250	0.242	3.3	50.27	49.73	1.011

the orbital energy difference of $\delta\varepsilon$. Considering merely the variation of the structural data with temperature has virtually no influence on the calculated quadrupole splitting (last row of Table 4). Assuming next a splitting of 1100 cm^{-1} between the two e_g-like orbitals, it is seen from the results in the fifth row of Table 4 that only the high-temperature behavior is being properly described: especially between 80 K and room temperature a decrease between 0.15 and 0.19 mm s^{-1} (this work) or 0.19 mm s^{-1} (Amthauer et al. 1976) is observed, whereas the calculated decrease of about 0.04 mm s^{-1} is significantly smaller. A possible interpretation of this discrepancy may be that the temperature dependence of the quadrupole splitting at low temperatures is affected by vibronic coupling effects as has been observed, e.g., in siderite (Nagy and Dezsi 1973; Price 1978) and ferrous fluosilicate (Price 1987), while only at more elevated temperatures does the thermal occupation of the d_{xy}-orbital become dominating. Allowing, thus, a linear temperature dependence (Srivastava 1984) of about 0.07 mm s^{-1} per 100 K due to vibronic coupling in order to reproduce the low-temperature behavior, a decrease in the quadrupole splitting by about 0.5 mm s^{-1} in the range from 80 to 800 K has to be assigned to this mechanism. Consequently, thermal occupation of the excited orbitals should contribute about another 0.5 mm s^{-1}, implying a separation of the two spin-down e_g-like orbitals between 1400 cm^{-1} and 1500 cm^{-1} (cf. sixth row of Table 4). On the other hand, the IR and Raman spectra in the region between about 1200 and 4500 cm^{-1} are featureless. Altogether, the conclusive interpretation of the temperature dependence of the quadrupole splitting, and thus the separation between the d_{z^2}- and d_{xy}-orbitals, requires more experimental data at elevated temperatures.

In the next step of the calculations, the dependence of the spectroscopic data upon the various garnet structures is investigated. To this end, 185-atom clusters are constructed for the model Pyr, Alm, Spe, and Gro structures where the central X-site in Pyr and Gro is occupied with Fe^{II}, while all other dodecahedra contain Mg and Ca, respectively. For Alm and Spe two sets of calculations have been performed, viz., (1) the central X-site is occupied with Fe^{II} and all other dodecahedra with Mg, and (2) in addition to the central X site, the four edge-sharing dodecahedra (cf. Fig. 4) are occupied with Fe^{II} and Mn^{II}, respectively. In the second case, the quadrupole splittings become larger by 0.08 and 0.05 mm s^{-1}, respectively, whereas the calculated d–d excitation energies get smaller between 100 and 300 cm^{-1}. Since the differences between (1) and (2) are within the estimated accuracy of 5–10% for this type of calculation, the second variant will not be considered further. The calculated hyperfine parameters and the d–d excitation energies of the spin-down 3d-orbitals for Fe^{II} in the dodecahedral X-site, based on the experimentally determined X-ray structures at 100 K, are listed in Table 5. While the ordering of the d-orbitals is the same in all cases, and the splitting of the two e_g-like orbitals decreases only by about 200 cm^{-1}, the splitting of the t_{2g}-like orbitals continuously decreases from 3847 cm^{-1} in model Pyr down to 3461 cm^{-1} in Spe and 2581 cm^{-1} in Gro, and the overall splitting

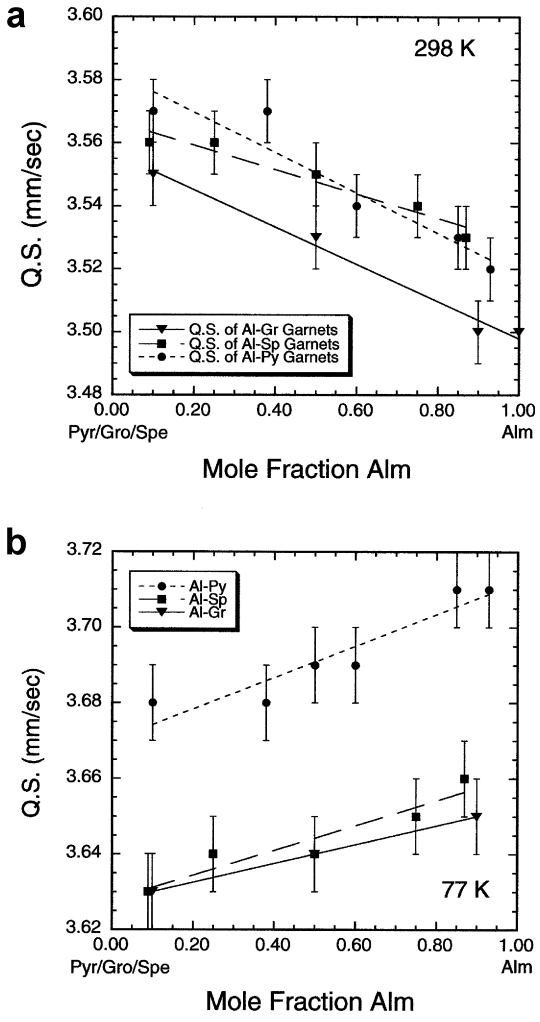

Fig. 2a, b Quadrupole splittings for the three almandine-containing binary solid solutions at 298 and 77 K, respectively. The errors are $\pm$ 0.01 mm s^{-1}

decreases from 8832 cm^{-1} in Pyr to 5323 cm^{-1} in Gro. This behaviour reflects, on one hand, the increase in the Fe–O distances from 2.196 and 2.334 Å in model Pyr to 2.321 and 2.483 Å in Gro (second column in Table 5). On the other hand, such a trend in the d–d excitation energies is not confirmed experimentally. Whereas

Table 3 Orbital energies (in cm^{-1}) of the spin-down Fe(3d)-orbitals relative to $3d_{z^2}$ and quadrupole splittings for almandine clusters of different size

No. of atoms	d_{xy}	d_{yz}	$d_{x^2-y^2}$	d_{xz}	$\Delta E_Q(\eta)$
9	669	2170	2855	3662	−3.628(0.08)
23	1186	1516	3476	7783	−3.918(0.20)
55	1226	3597	5210	7324	−3.980(0.04)
67	1602	4218	5694	6799	−3.732(0.01)
99	1703	4041	5928	7340	−3.641(0.01)
115	1703	4121	6009	7469	−3.621(0.01)
125	1663	4331	6017	7203	−3.585(0.02)
141	1647	4170	6081	7743	−3.558(0.06)
153	1591	4775	6348	7485	−3.624(0.04)
161	1631	4363	6259	7880	−3.697(0.02)
173	1671	4525	6420	8082	−3.640(0.00)
185	1687	4363	6299	7928	−3.665(0.03)
exp	(1100)	4350	5850	7600	−3.654

the values for almandine are in reasonable agreement with the experimental data, e.g., about 7650 cm^{-1} for the splitting between the d_{z^2}- and d_{xz}-orbitals, the corresponding measured values are about 7900 cm^{-1} for pyrope-rich garnets, 7860 cm^{-1} for spessartine-rich garnets, and about 8200 cm^{-1} for grossular-rich garnets (White and Moore 1972; Geiger and Rossman 1994). In particular, the last value is hardly comprehensible in view of the fact that the average Fe–O distance increases by 0.137 Å from model Pyr to Gro. Since the experimental structural data were obtained for Fe^{II}-poor samples, this discrepancy must be assigned to substantial local relaxation of the dodecahedra when Fe^{II} is substituting for the corresponding X^{II} cation. It is, however, difficult to calculate quantitatively the extent of such substitutional distortions (see Bosenick et al. 2000). A useful indication could be provided by a study of temperature- and pressure-dependent changes of the *d–d* excitation energies. Calculated orbital energies for almandine between 100 and 500 K exhibit variations between 150 and 200 cm^{-1} except for the lowest d_{xy}-orbital (results not shown). Measurements at 101 kbar yield an increased splitting of 600 cm^{-1} for d_{xz}, 900 cm^{-1} for $d_{x^2-y^2}$, and 1134 cm^{-1} for d_{yz} (Smith and Langer 1983), demonstrating considerable compression of the dodecahedron.

Unlike the *d–d* excitation energies, the calculated hyperfine parameters are almost identical for model Pyr, Alm, and Spe (last two columns of Table 5), in accordance with experimental findings, and the moderately larger changes for model Gro can be attributed to the distinctly longer Fe–O distances. Such a result is comprehensible when remembering that the ligand and covalence contributions to the quadrupole splitting are negligible. This is also reflected in the charge distribution within the first coordination sphere of iron (Table 6). The effective charges of the oxygens are nearly identical and the absolute values are relatively small compared with the formal charge or oxidation number of −2. It is therefore not surprising that the ligand contribution from the first coordination sphere is small. Furthermore, as can be expected in view of the relatively large bond distances, the overlap populations are quite small. This indicates a correspondingly small covalent contribution to the total Fe–O bond, as do the spin densities in the Fe(3*d*)-shell (last column in Table 6) that are close to the ideal value of 4. Since the quadrupole splitting is determined solely by the 3*d*-shell occupation, the analysis of the origin of the efg may be restricted to the 3*d*-valence contribution which is, in the principal axes system of the efg tensor, approximately proportional to the anisotropy Δn_d, Eq. (3), of the Fe(3*d*)-shell occupation. The occupation numbers of the ten 3(*d*)-orbitals in Table 7 demonstrate first that the spin-up orbitals do not contribute to the efg. This reflects the near-spherical symmetry of the charge distribution of a closed shell as provided by the five spin-up 3*d*-electrons. Secondly, the value of $\Delta n_{d\downarrow}$ mainly reflects the character of the d_{z^2}-orbital that is the only occupied spin-down MO with predominant iron character. This value is only slightly modified due to the covalent admixtures of the other four formally empty spin-down 3*d*-orbitals to the occupied ligand molecular orbitals. Altogether, since the electric-field gradient is determined by the anisotropy of the 3*d* shell that is only weakly influenced by geometrical and chemical changes, measured quadrupole splittings cannot distinguish between garnet solid solutions within the series Pyr, Alm, Spe, and Gro.

The same is true for the isomer shift, δ, related to the electronic density, $\rho(0)$, at the nucleus. Since, under otherwise equal conditions, $\rho(0)$ generally decreases, i.e., δ increases, with increasing distance, and an increasing Fe–O bond distance is often accompanied with a larger ionicity of the bond, changes in the magnitude of δ can, in principle, measure differences in the type of bonding between Fe^{II} and oxygen. This correlation between bond distances and isomer shifts is reflected in the respective calculated δ-values (Table 5), but the differences (except for Gro) are too small to be considered as significant. A more direct comparison, of course, is provided by the analysis of the computed charge density distribution (Table 6). Indeed, the effective charge of iron increases from model Pyr to Spe while the overlap population between Fe and O decreases and, additionally, the population of the *d* shell decreases while its spin density increases. All these results indicate an increasing ionic character of the Fe–O bonds. On the other hand, the results for model Gro do not follow this trend, except for the overlap population.

Discussion of spectra

Bonding and X-site distortion

The remarkably constant isomer shift values across all three garnet solid solutions at both temperatures, 77 and 298 K, indicate that the type of bonding of Fe^{II} with its

Table 4 Temperature dependence of the quadrupole splitting of Fe^{II} in the dodecahedral position for model pyrope and almandine structures

T(K)	Alm(exp)[a]	Alm(exp)	pyr(exp)[b]	alm(cal)[d]	alm(cal)[e]	Alm(cal)[f]
77–80	−3.65	−3.66[b]	−3.65	−3.665	−3.665	−3.665
293–295	−3.50	−3.47[b]	−3.54	−3.624	−3.652	−3.659
420	−3.36	–	–	−3.483	−3.594	−3.656
473	–	–	−3.40	−3.396	−3.550	–
500	–	–	–	−3.344	−3.520	−3.654
681	–	–	−3.11	−2.971	−3.275	–
800	–	−2.70[c]	–	−2.721	−3.081	–

[a] Geiger et al. 1992
[b] Amthauer et al. 1976
[c] Lyubutin et al. 1970
[d] Based on an assumed e_g-splitting of 1100 cm^{-1}
[e] Based on an assumed e_g-splitting of 1400 cm^{-1}
[f] Geometrical changes only accounted for

Table 5 Fe–O distances (in Å), orbital energies (in cm^{-1}) of the spin-down Fe(3*d*)-orbitals relative to $3d_{z^2}$, and calculated hyperfine parameters (in mm s^{-1}) for model Pyr, Alm, Spe, and Gro structures at 100 K

	d(Fe–O)	d_{xy}	d_{yz}	$d_{x^2-y^2}$	d_{xz}	ΔE_Q	δ
Pyr	2.196, 2.334	1737	4985	6912	8832	−3.671	1.394
Alm	2.220, 2.363	1687	4363	6299	7928	−3.665	1.400
Spe	2.245, 2.399	1647	3750	5727	7211	−3.659	1.406
Gro	2.321, 2.483	1578	2742	4444	5323	−3.574	1.451

Table 6 Effective charges *Q*, overlap populations *P*, *d*-shell occupation *n* and *d*-shell spin-density *m* of Fe^{II} in the dodecahedral X-site for model Pyr, Alm, Spe, and Gro structures at 100 K

Model	*Q*(Fe)	$Q(O_1)$	$Q(O_2)$	$P(FeO_1)$	$P(FeO_2)$	*n*(Fe3*d*)	*m*(Fe3*d*)
Pyr	0.712	−0.479	−0.499	0.127	0.110	6.310	3.650
Alm	0.784	−0.477	−0.499	0.120	0.101	6.293	3.670
Spe	0.828	−0.478	−0.511	0.117	0.094	6.280	3.686
Gro	0.799	−0.457	−0.498	0.107	0.085	6.329	3.646

Table 7 Occupation numbers and anisotropy of the spin-up and spin-down 3*d* shell of Fe^{II} in the dodecahedral X-site for model Pyr, Alm, Spe, and Gro structures at 100 K

Model	n_{z^2}	n_{xy}	n_{yz}	$n_{x^2-y^2}$	n_{xz}	Δn_d
Pyr(up)	0.998	0.998	0.996	0.994	0.994	−0.001
Pyr(down)	0.996	0.032	0.054	0.085	0.123	−0.968
Alm(up)	0.998	0.998	0.997	0.994	0.995	−0.002
Alm(down)	0.995	0.031	0.051	0.082	0.119	−0.967
Spe(up)	0.998	0.998	0.997	0.995	0.996	−0.002
Spe(down)	0.995	0.031	0.048	0.080	0.117	−0.966
Gro(up)	0.999	0.999	0.998	0.996	0.997	−0.001
Gro(down)	0.993	0.030	0.041	0.075	0.107	−0.962

surrounding oxygen ligands does not change measurably as a function of garnet composition. There exist also no significant differences between the measured and calculated quadrupole splittings for the synthetic solid solutions, as well as between those recorded on natural garnets (e.g., Amthauer et al. 1976). While, in a first-order analysis, the minor variations in the quadrupole splitting values across a given garnet binary would lead one to conclude that distortion of the $Fe^{II}O_8$-dodecahedra does not depend upon composition, such an interpretation is not supported by NIR measurements (Geiger and Rossman 1994). Indeed, the NIR spectra provide a better measure of local distortions, because the crystal field splitting 10 Dq is much more sensitive against changes in the Fe–O bond lengths. Nevertheless, the variations of the Fe^{II} *d–d* energies in garnet solid solutions remain relatively small, at least compared with what is expected according to both ligand-field theory and the electronic structure calculations discussed above. Therefore, the discrepancy between measured and calculated *d–d* energies suggests that Fe–O bond lengths remain relatively constant across the different solid solutions.

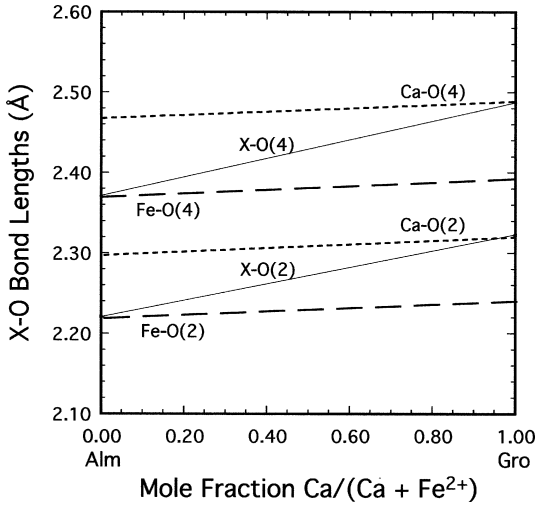

Fig. 3 The two crystallographically independent (Ca,Fe)–O bond lengths in Alm–Gro solid solutions. The *different dashed lines* show possible approximate Fe–O and Ca–O bond lengths as a function of composition. They represent the state of alternating bonds and are considered as a reasonable description for garnet solid solutions. The *thin straight lines* represent the case without local structural relaxation (virtual crystal approximation). Effects related to the excess volume properties are considered to be secondary in nature and have been ignored

The data support the crystal-chemical model that the Fe–O bonds, and probably the other ones as well (i.e., Ca–O, Mn–O, Mg–O), retain to a large degree the length and character they have in the respective end members. This behavior is most consistent with the state of alternating bonds, which is, in turn, associated with strong local structural relaxation (Martins and Zunger 1984; Urusov 2001). Possible bond lengths for the Alm–Gro solid solution, for example, are shown schematically in Fig. 3. Such a behavior has been documented for $Ga_{1-x}In_xAs$ semiconductor solid solutions via EXAFS studies (Mikkelsen and Boyce 1983). In contrast, Ungaretti et al. (1995) concluded, based on a structural analysis of many garnets refined by single-crystal X-ray diffraction methods, that the chemical bonds in Mg-, Fe^{II}-, Mn^{II}-rich aluminosilicate garnets are largely ionic in character, while the bonds in Ca-rich garnets exhibit a more covalent nature expressed, e.g., by a smaller distortion of the SiO_4 tetrahedra. However, such an approach to understand the bonding in garnet is not supported by the calculated charge density distribution: neither the charges and overlap populations at the X-site (cf. Table 6), nor those of the SiO_4-tetrahedra (Table 8) change significantly in going from model Pyr to Gro. Especially within the latter, the charges and overlap populations show only marginal differences and the same is true for the AlO_6-octahedra (data not shown). Moreover, the charge distributions at the X-site are expected to become even more similar to each other due to the structural relaxation that is necessary to explain the relatively small variations in the NIR spectra. Hence, the nature of the chemical bonds should be similar in all of the four investigated garnet structures.

Table 8 Si–O distances (in Å), effective charges Q and overlap populations P within the SiO_4 tetrahedra for model Pyr, Alm, Spe, and Gro structures at 100 K

Model	d(Si–O)	Q(Si)	Q(O)	P(SiO)
Pyr	1.634	0.519	−0.497	0.752
Alm	1.636	0.505	−0.492	0.755
Spe	1.639	0.484	−0.503	0.758
Gro	1.646	0.500	−0.482	0.750

Table 9 Contributions to the overlap populations of the iron oxygen bonds for model Pyr, Alm, Spe, and Gro structures at 100 K

		Pyr	Alm	Spe	Gro
$Fe–O_1$	4sp	0.117	0.110	0.106	0.095
	3d↑	−0.016	−0.015	−0.013	−0.008
	3d↓	0.026	0.025	0.024	0.020
$Fe–O_2$	4sp	0.107	0.098	0.091	0.082
	3d↑	−0.010	−0.009	−0.008	−0.005
	3d↓	0.013	0.012	0.011	0.008

It is also instructive to examine the bonding modes of iron in more detail. Decomposing the Fe–O overlap populations into the contributions from the 4sp-, the $3d_{\uparrow}$- and the $3d_{\downarrow}$-orbitals, respectively, shows that the covalent part of the Fe–O bond is almost exclusively determined by the 4sp-orbitals (Table 9). The $3d_{\uparrow}$-orbitals yield a small antibonding (negative) contribution corresponding to the fact that both the bonding and the antibonding spin-up linear combinations of the $Fe(3d_{\uparrow})$- and the $O(2p_{\uparrow})$-orbitals are occupied. Accordingly, the effective contribution of the 3*d*-electrons to the bond is an order of magnitude smaller compared to the 4*sp*-electrons. Analogous results have been obtained for iron in chlorite (Lougear et al. 2000), epidote (Grodzicki et al. 1999), and Fe-bearing lazulites (Grodzicki et al. 2003). Although the covalent contribution constitutes a relatively small part of the total Fe–O bond at the X-site in garnets, these results suggest that the discussion of crystal field stabilization energies solely in terms of the *d*-electrons needs careful justification.

Measurable changes in quadrupole splitting parameters have been observed in other silicate solid solutions, e.g., for octahedral Fe^{II} in synthetic pyroxenes (Dowty and Lindsley 1973; Dollase and Gustafson 1982). For diopside–hedenbergite $(Ca,Mg)Si_2O_6$–$(Ca,Fe)Si_2O_6$ solid solutions the quadrupole splittings change from 1.85 (2) to 2.19 (1) $mm^{-1}s$ going from diopside- to hedenbergite-rich compositions, whereas the isomer shift values remain constant at 1.18(1) mm s^{-1} at 298 K (Dollase and Gustafson 1982). The results from the hedenbergite–ferrosilite ($Fe_2Si_2O_6$) binary are particularly relevant for this study on garnets, because Ca–Fe exchange occurs on the M2 site, which is a large, highly distorted site with seven to eight oxygen nearest neighbors. Here, only minor changes in the quadrupole splitting and isomer shift are associated with mixing on the M2 site (Dowty and Lindsley 1973). The smaller and more regular octahedral M1 site, on the other hand, is associated with measurable changes in the quadrupole splitting values (2.22 to 2.49 mm s^{-1}), although it is totally occupied by Fe^{II} across the join. Together with the results for the eightfold-coordinated X-site in garnets it appears, therefore, that with increasing polyhedral coordination number the quadrupole splitting ceases to be a sensitive measure of Fe^{II}-site distortion in silicates. The physical basis for this conclusion is delivered by the theoretical analysis of the efg in the preceding section: increasing coordination number is connected with increasing metal–ligand distances. This leads, in turn, to negligible covalence and ligand contributions to the efg, and the then dominating 3*d*-shell anisotropy is only weakly influenced by structural and chemical changes.

Doublet asymmetry and Fe^{II} vibrational behavior

It can be seen in the spectra of the Alm–Pyr and Alm–Spe binaries that the shape of the two lines of the Fe^{II} doublet are not identical but exhibit some degree of asymmetry. The spectra from the Alm–Gro binary, on the other hand, show more symmetric doublets. For the former binaries, as in the case of end-member Alm (Geiger et al. 1992), the high-velocity line is slightly narrower and more intense than the low-velocity line (Fig. 1a,b; Tables 1, 2). The line widths are, however, in general, not significantly different than those observed in end-member Alm. It is observed that (1) the area of the low-velocity line is almost always slightly greater than that of the high-velocity line and (2) the line areas for all three solid solutions do not change systematically or greatly as a function of garnet composition at 298 or 77 K. This is shown in Tables 1 and 2 listing the areas of the individual absorption lines and their area ratios.

The asymmetry of the lines can be expressed as a ratio of their areas (Geiger et al. 1992). In the ideal case where (1) no different next-nearest neighbor dodecahedral cation interactions are present (i.e., local compositional differences), giving rise to their own intrinsic quadrupole splitting doublets, and (2) no anisotropic recoil-free fraction would occur, the area ratio should be 1.0. However, because the differences in areas between the two lines are very small, so that a quantitative measure of area ratios is difficult to obtain, it is preferable to express the observed asymmetry differences in the two resonance lines by a doublet asymmetry parameter, DAS. It is based solely on the line widths (Tables 1 and 2), because these can be measured precisely. The following observations for the three solid solutions are then in order. The DAS parameter and the individual line widths show no marked variations across the Alm–Gro binary at 298 and 77 K. For the Alm–Spe binary, the line widths at 298 K appear to increase a little with increasing Spe component and they also become broader with decreasing temperature. The line widths of the low-velocity line at 298 K show the largest changes, which is reflected in the DAS parameter

(Tables 1, 2). The DAS parameter increases with increasing Spe content at 298 and 77 K and is greater at the lower temperature for each composition. Along the Alm–Pyr binary, the DAS parameter also increases with decreasing Alm component, but not in such a clear and systematic manner as in the case of Alm–Spe garnets. The variations in DAS at 298 K are a result of a general small decrease in the line widths of the high-velocity line, while the low-velocity line maintains an approximately constant half-width. The DAS parameter increases with decreasing temperature as in Alm–Spe garnets.

The question now arises: what is the reason for the variations in Fe^{II} doublet asymmetry or lack of it as a function of garnet composition? Texture effects can be ruled out, because garnet has poor cleavage and, moreover, spectra recorded where the absorber was fixed at an angle of 54°44′ with respect to the incident gamma-ray show no differences compared to those measured perpendicular to the incident radiation. Magnetic relaxation (Amthauer et al. 1976) is also unlikely to play an important role, inasmuch as the doublet asymmetry does not always increase with decreasing temperature and it is not a function of composition, i.e., Alm–Gro. One possible explanation is through the phenomenon of anisotropic recoil-free fraction (Geiger et al. 1992). Greater doublet asymmetry, versus that observed in end-member Alm in this case, should be associated with greater anisotropic vibration of Fe^{II} with changing garnet composition. To address this issue properly, the geometry and distortion of the dodecahedral X-site as a function of composition must be considered along with the possible vibrational behavior of the Fe^{II} cation. It has been shown from X-ray diffraction results on the end-member aluminosilicate garnets that the X-site cations vibrate in a strongly anisotropic manner, whereby their respective amplitudes of vibration depend upon the size and mass of the cations (Armbruster and Geiger 1993; Geiger and Armbruster 1997). It was shown, in addition, that the size and degree of diffraction-based dodecahedral X-site distortion in solid solutions increase with increasing average size of the X-site cation (Geiger and Feenstra 1997). This is relevant, because the degree of anisotropic vibration of an X-cation should increase with both increasing size and distortion of the dodecahedral site. Both should be greater with increasing Spe or Gro substitution in a solid solution relative to end-member Alm, because Mn^{II} and Ca are larger than Fe^{II}.

Hence, Fe^{II} cations could potentially vibrate in an increasingly anisotropic manner with increasing Spe and/or Gro substitution. The effect should be most pronounced in Alm–Gro, because the ionic radius of Ca is distinctly larger than that of Mn^{II} (1.12 vs. 0.96 Å in eight fold coordination). The observed increase in Fe^{II}-doublet asymmetry in Alm–Spe garnets with increasing Spe substitution (Fig. 1a, b) is consistent with such an explanation. The degree of asymmetry decreases, however, with increasing temperature from 77 to 298 K, contrary to the expectation in the case of an anisotropic recoil free fraction. Moreover, the spectra of the Alm–Gro garnets, do not show the expected variations in doublet asymmetry with changing composition. The Fe^{II} doublet remains essentially unchanged across this join. In the case of Alm–Pyr garnets, increasing doublet asymmetry occurs with increasing Pyr substitution. Therefore, anisotropic Fe^{II} vibration should increase with increasing Pyr content in garnet, but this is at variance with the crystal chemistry of these garnets, because Mg is smaller than Fe^{II}.

Concluding, the variations in the Fe^{II} doublet asymmetries for the three binaries cannot be reconciled with the diffraction-average crystal-chemical properties. They do not provide a proper structural description of the local Fe-dodecahedral sites. Variations in the vibrational properties of Fe^{II} and any associated anisotropic recoil-free fraction effects cannot explain the experimental data. Variations in doublet asymmetry or its lack thereof in the solid solutions must have another cause.

The question of short-range cation ordering

The presence or absence of short-range X-site cation order and its possible effect on the Mössbauer spectra is difficult to analyze in both theory and experiment. On the theoretical side, it is nearly impossible to show via quantum mechanical calculations the effect of short-range ordering on the localized electric-field gradients, because the degree of local distortion cannot be determined with certainty. Therefore, any calculation modeling short-range ordering on the X-site cannot be considered as conclusive. The experimental spectra are also difficult to analyze and interpret. If short-range order occurs in these synthetic garnets, the presence of different local cation configurations and their effect on the hyperfine parameters must be small considering the narrowness of the line widths, which for the most part are less than 0.30 mm s^{-1}. In order to address this issue, it is necessary to first consider the linkage of the dodecahedra so as to be able to formulate a description of possible interactions between nearest-neighbor X-site cations. Figure 4 shows the edge-sharing arrangement between neighboring dodecahedra in the garnet structure. Since the SiO_4 tetrahedra and AlO_6 octahedra do

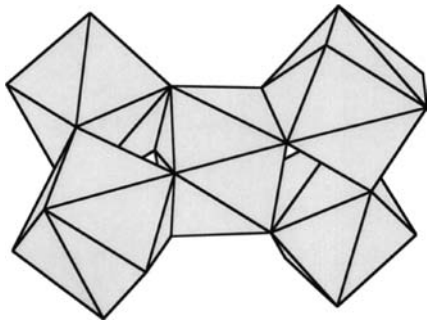

Fig. 4 The edge-sharing relationship between neighboring dodecahedra in the garnet structure. Every dodecahedron shares four edges with other dodecahedra

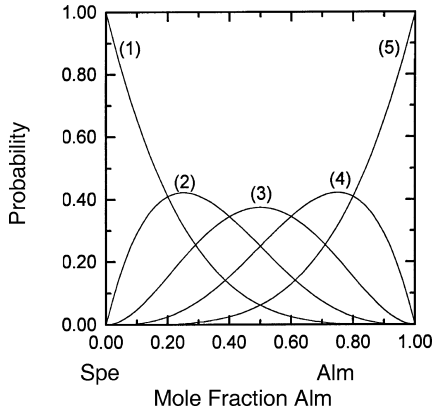

Fig. 5 Calculated probabilities for the five different random first-sphere cation configurations that can occur locally around a Fe^{II} dodecahedron as a function of garnet composition along the Al–Sp binary, which is used as an example. **1** corresponds to the configuration Mn–Mn–Mn–Mn; **2** Fe–Mn–Mn–Mn; **3** Fe–Fe–Mn–Mn; **4** Fe–Fe–Fe–Mn, **5** Fe–Fe–Fe–Fe

not change greatly upon X-cation exchange, any changes in the spectra are considered as originating primarily from variations in the neighboring X-site cation configurations (i.e., first-sphere interactions). Higher-order interactions are considered not to affect the electric-field gradient around a given Fe^{II} nucleus. Thus, five different local configurations are possible. For example, in Alm–Spe garnets they are Mn–Mn–Mn-Mn, Fe–Mn–Mn–Mn, Fe–Fe–Mn–Mn, Fe–Fe–Fe–Mn, and Fe–Fe–Fe–Fe. Their calculated probabilities for a statistically random cation distribution across the binary are illustrated in Fig. 5. In principle, each local configuration should be characterized by its own quadrupole doublet. In the hypothetical case of a 50:50 solid solution line-broadening relative to end-member almandine would be expected, resulting from the overlap of five resonant absorption doublets of varying intensity. In the hypothetically extreme case, separate absorption doublets characteristic of each local configuration and its concentration, each with different hyperfine parameters, would occur, which is clearly not the case. On the other hand, with short-range order, the spectra could be expected to show systematic variations in the hyperfine parameters, in doublet asymmetry or line broadening. This is the case in the spectra of pyroxene solid solutions (e.g., Dowty and Lindsley 1973; Seifert 1983).

Among the three different garnet solid solutions, the Alm–Spe binary shows the largest and most systematic variations in the Fe^{II} doublet. Here, for example, the line widths become measurably broader with decreasing temperature. This lends some credence to the possibility that these Alm–Spe garnets are characterized by some degree of short-range order. However, due to the relative narrowness of the absorption lines and hence, strong overlapping of different doublets, no meaningful fits can be produced (Dollase 1975). Hence, the question of short-range order cannot be answered conclusively with the present spectra and the fitting algorithms employed herein. Summarizing, ^{57}Fe Mössbauer spectroscopy does not appear be a suitable method for investigating the effect of short-range order in aluminosilicate garnet solid solutions. The resolution afforded by using the Si nucleus as a probe in ^{29}Si NMR spectroscopy is clearly better (Bosenick et al. 1995, 1999), but unfortunately the method is not suitable for iron-containing compounds.

Conclusions

The investigation of three binary aluminosilicate garnet solid solutions by ^{57}Fe Mössbauer spectroscopy and by electronic structure calculations in the local spin density approximation has shown that local structural relaxation must take place with the substitution of differently sized X-site cations, in order to reconcile calculated and measured Fe^{II} *d–d* excitation energies. Accordingly, the element-specific X–O bonds are better described by the state of alternating bonds and not by the virtual crystal approximation. This conclusion is in agreement with structure-modeling results obtained from calculations on garnet solid solutions using empirical pair potentials (Bosenick et al. 2001). They show that structural relaxation occurs upon exchange of X-site cations in garnet and that they are important in controlling the macroscopic physical properties such as the thermodynamic mixing properties. Mössbauer hyperfine parameters do not however, exhibit, variations that are significant enough to discriminate between the different solid solutions. The physical basis for this result is the high coordination number connected with the large Fe–O distances. This, in turn, leads to negligible contributions of the cationic neighbors to the electric-field gradient and to the electron density at the nucleus. Thus, Mössbauer spectroscopy probably cannot offer the possibility to investigate short-range order or to be used for characterizing local structural distortions in aluminosilicate garnets. The analysis of the calculated charge density distribution does not support the view that the chemical bonds in grossular-type garnets are more covalent than in the pyralspites.

Acknowledgements We would like to thank Anne Feenstra for the donation of the Alm–Spe garnets and Henning Voigtländer, who measured some of the spectra. This research has been funded by the Deutsche Forschungsgemeinschaft (DFG), grants Ge 659/8-2/8-3 and De 412/26-3, as part of a Schwerpunktprogramm, and by the Austrian Fonds zur Förderung der wissenschaftlichen Forschung (FWF), grant no. P12424-GEO. All calculations were carried out at the Research Institute of Software Technology (RIST) of the TechnoZ in Salzburg.

References

Akai H, Blügel S, Zeller R, Dederichs PH (1986) Isomer shifts and their relation to charge transfer in dilute Fe alloys. Phys Rev Lett 56: 2407–2410

Amthauer G, Annersten H, Hafner SS (1976) The Mössbauer spectrum of ^{57}Fe in silicate garnets. Z Kristallog 143: 14–55

Armbruster T, Geiger CA (1993) Andradite crystal chemistry, dynamic X-site disorder and structural strain in silicate garnets. Eur J Mineral 5: 59–71

Armbruster T, Geiger CA, Lager GA (1992) Single-crystal X-ray structure study of synthetic pyrope almandine garnets at 100 and 293 K. Am Mineral 77: 512–521

Blaha P, Schwarz K, Faber W, Luitz J (2000) Calculations of electric field gradients in solids: how theory can complement experiment. Hyperfine Int 126: 389–395

Bosenick A, Geiger CA, Schaller T, Sebald A (1995) A ^{29}Si MAS NMR and IR spectroscopic investigation of synthetic pyrope–grossular garnet solid solutions. Am Mineral 80: 691–704

Bosenick A, Geiger CA, Phillips B (1999) Local Ca–Mg distribution of Mg-rich pyrope–grossular garnets synthesized at different temperatures revealed by ^{29}Si NMR MAS spectroscopy. Am Mineral 84: 1422–1433

Bosenick A, Dove MT, Geiger CA (2000) Simulation studies on the pyrope–grossular garnet solid solution. Phys Chem Miner 27: 398–418

Bosenick A, Dove MT, Heine V, Geiger CA (2001) Scaling of thermodynamic mixing properties in solid solution minerals. Phys Chem Miner 28: 177–187

Burns RG (1993) Mineralogical applications of crystal field theory, 2nd ed., Cambridge University Press, Cambridge, UK

Dollase WA (1975) Statistical limitations of Mössbauer spectra fitting. Am Mineral 60: 257–264

Dollase WA, Gustafson WI (1982) ^{57}Fe Mössbauer spectral analysis of the sodic clinopyroxenes. Am Mineral 67: 311–317

Dowty E, Lindsley DH (1973) Mössbauer spectra of synthetic hedenbergite-ferrosilite pyroxenes. Am Mineral 58: 850–868

Dufek P, Blaha P, Schwarz K (1995) Determination of the nuclear quadrupole moment of ^{57}Fe. Phys Rev Lett 75: 3545–3548

Duff KJ (1974) Calibration of the isomer shifts for ^{57}Fe. Phys Rev (B)9: 66–72

Eriksson O, Svane A (1989) Isomer shifts and hyperfine fields in iron compounds. J Phys Cond Matter 1: 1589–1599

Evans BJ, Sergent EW Jr (1975) ^{57}Fe NGR of Fe phases in "magnetic cassiterites". Contrib Min Petrol 53: 183–194

Geiger CA (1993) ^{57}Fe-Mössbauer spectroscopy of almandine–spessartine garnets. EOS 74: 676

Geiger CA (1998) A powder infrared spectroscopic investigation of garnet binaries in the system $Mg_3Al_2Si_3O_{12}$–$Fe_3Al_2Si_3O_{12}$–$Mn_3Al_2Si_3O_{12}$–$Ca_3Al_2Si_3O_{12}$. Eur J Mineral 10: 407–422

Geiger CA (1999) Thermodynamics of $(Fe^{2+},Mn^{2+},Mg,Ca)_3Al_2Si_3O_{12}$ garnet: an analysis and review. Mineral Petrol 66: 271–299

Geiger CA, Armbruster T (1997) $Mn_3Al_2Si_3O_{12}$ spessartine and $Ca_3Al_2Si_3O_{12}$ grossular garnet: structural dynamic and thermodynamic properties. Am Mineral 82: 740–747

Geiger CA, Feenstra A (1997) Molar volumes of mixing of almandine-pyrope and almandine–spessartine garnets and the crystal chemistry and thermodynamic mixing properties of the aluminosilicate garnets. Am Mineral 82: 571–581

Geiger CA, Rossman GR (1994) Crystal field stabilization energies of almandine–pyrope and almandine–spessartine garnets determined by FTIR near-infrared measurements. Phys Chem Miner 21: 516–525

Geiger CA, Newton RC, Kleppa OJ (1987) Enthalpy of mixing of synthetic almandine-grossular and almandine–pyrope garnets from high-temperature solution calorimetry. Geochim Cosmochim Acta 51: 1755–1763

Geiger CA, Winkler B, Langer K (1989) Infrared spectra of synthetic almandine-grossular and almandine–pyrope garnet solid solutions: evidence for equivalent site behavior. Mineral Mag 53: 231–237

Geiger CA, Lottermoser W, Amthauer G (1990) A temperature dependent ^{57}Fe Mössbauer study of synthetic almandine–grossular and almandine–pyrope garnets: a comparison. 3rd International Symposium of Experimental Mineralogy, Petrology and Geochemistry Edinburgh, U.K, p 11

Geiger CA, Armbruster T, Lager GA, Jiang K, Lottermoser W, Amthauer G (1992) A combined temperature-dependent ^{57}Fe Mössbauer and single-crystal X-ray diffraction study of synthetic almandine: evidence for the Goldanskii-Karyagin effect. Phys Chem Miner 19: 121–126

Grodzicki M (1980) A self-consistent-charge Xα method I. Theory. J Phys (B)13: 2683–2691

Grodzicki M (1985) Theorie und Anwendungen der Self-Consistent-Charge-Xα Methode. Thesis of Habilitation, Universität Hamburg

Grodzicki M, Amthauer G (2000) Electronic and magnetic structure of vivianite: cluster molecular orbital calculations. Phys Chem Miner 27: 694–702

Grodzicki M, Männing V, Trautwein AX, Friedt JM (1987) Calibration of isomer shifts and quadrupole coupling constants for ^{119}Sn, ^{127}I and ^{129}I as derived from SCC-Xα calculations and Mössbauer measurements. J Phys (B)20: 5595–5625

Grodzicki M, Heuss-Assbichler S, Amthauer G (2001) Mössbauer investigations and molecular orbital calculations on epidote. Phys Chem Miner 28: 675–681

Grodzicki M, Redhammer GJ, Amthauer G, Schünemann V, Trautwein AX, Velickov B, Schmid-Beurmann P (2003) Electronic structure of Fe-bearing lazulites. Am Mineral 88: 481–488

Jansen N, Spiering H, Gütlich P, Stahl D, Kniep R, Eyert V, Kübler J, Schmidt PC (1992) Mössbauer-Spektroskopie und Elektronenstrukturberechnungen an Nitridoferraten(III): $Li_3[FeN_2]$ und $Ba_3[FeN_3]$. Angew Chemie 104: 1632–1634

Keutel H, Käpplinger I, Jäger EG, Grodzicki M, Schünemann V, Trautwein AX (1999) Structural, magnetic and electronic properties of a pentacoordinated intermediate-spin (S = 3/2) iron(III) complex with a macrocyclic $[N_4]^{2-}$ ligand. Inorg Chem 38: 2320–2327

Kolesov B, Geiger CA (1998) Raman spectra of silicate garnets. Phys Chem Miner 25: 142–151

Lauer S, Marathe VR, Trautwein AX (1979) Sternheimer shielding using various approximations. Phys Rev (A)19: 1852–1861

Lottermoser W, Steiner K, Scharfetter G, Jiang K, Grodzicki M, Redhammer G, Amthauer G, Treutmann W (2002) The electric-field gradient in synthetic fayalite α-Fe_2SiO_4 at moderate temperatures. Phys Chem Miner 29: 112–121

Lougear A, Grodzicki M, Bertoldi C, Trautwein AX, Steiner K Amthauer G (2000) Mössbauer and molecular orbital study of chlorites. Phys Chem Miner 27: 258–269

Lyubutin IS, Dodokin AP (1971) Temperature dependence of the Mössbauer effect for Fe^{2+} in dodecahedral coordination in garnet. Sov Phys Crystallog 15: 1091–1092 (translated from Kristallografiya, 15: 1249–1250 (1970)

Lyubutin IS, Lyubutina LG (1971) A Mössbauer study of the spectrum of iron atoms in three crystallographically non-equivalent sites of the garnet structure. Sov Phys Crystallog 15: 708–710 (translated from Kristallografiya 15: 824–826 (1970)

Martins JL, Zunger A (1984) Bond lengths around isovalent impurities and in semiconductor solid solutions. Phys Rev (B)30: 6217–6220

Mikkelsen JC, Boyce JB (1983) Extended X-ray absorption fine structure study of $Ga_{1-x}In_xAs$ random solid solutions. Phys Rev (B)28: 7130–7140

Murad E, Wagner FE (1987) The Mössbauer spectrum of almandine. Phys Chem Miner 14: 264–269

Nagy DL, Dezsi I (1973) The anomalous temperature dependence of the Mössbauer linewidth of $FeCO_3$ (siderite). Sol State Comm 12: 749–751

Newman DJ, Price DC, Runciman WA (1978) Superposition model analysis of the near-infrared spectrum of Fe^{2+} pyrope–almandine garnets. Am Mineral 63: 1278–1281

Nieuwpoort WC, Post D, van Duijnen PT (1978) Calibration constant for ^{57}Fe Mössbauer isomer shifts derived from ab initio self-consistent-field calculations on octahedral FeF_6 and $Fe(CN)_6$ clusters. phys Rev (B)17: 91–98

Price DC (1978) Vibronic effects in Mössbauer spectra: the ^{57}Fe quadrupole splitting in $FeCO_3$. Austr J Phys 31: 397–420

Price DC (1987) Static and dynamic crystal-field effects in ferrous fluosilicate. Can J Phys 65: 1280–1293

Ray SN, Das TP (1977) Nuclear quadrupole interaction in the Fe^{2+} ion including many-body effects. Phys Rev (B)16: 4794–4804

Seifert F (1983) Mössbauer line broadening in aluminous orthopyroxenes: evidence for next-nearest-neighbors interactions and short-range order. Neues Jb Miner Abh 148: 141–162

Slater JC (1974) Quantum theory of molecules and solids, vol. 4, McGraw-Hill, New York

Smith G, Langer K (1983) High-pressure spectra up to 120 kbars of the synthetic garnet end members spessartine and almandine. N Jb Miner Mh: 541–555

Srivastava KKP (1984) Effect of the orbit-lattice interaction in Mössbauer studies: quadrupole splitting of $^{57}Fe(II)$ in $MgCO_3$. Phys Rev (B)29: 4890–4895

Ungaretti L, Leona M, Merli M, Oberti R (1995) Non-ideal solid solution in garnet: crystal-structure evidence and modeling. Eur J Mineral 7: 1299–1312

Urusov VS (2001) The phenomenological theory of solid solutions. In: Geiger CA (ed) Solid solutions in silicate and oxide systems. European Mineral Union, Notes in Mineralogy, vol. 3, pp. 121–153

van der Heyden M, Micklitz H, Bukshpan S, Longouche G (1987) Systematics in the ionization states of ^{57}Fe following the electron capture decay of ^{57}Co in different rare-gas matrices. Phys Rev (B)36: 38–43

White BW, Moore RK (1972) Interpretation of the spin-allowed bands of Fe^{2+} in silicate garnets. Am Mineral 57: 1692–1710

Zhang Q, Zhang Y, Wang D (1987) Isomer shift calibration of Fe nucleus by self-consistent all-electron LAPW band calculation. Commun Theor Phys 8: 139–151

View publication stats